Environmental Sciences Europe

RESEARCH Open Access

# Simulated solar light-driven photocatalytic degradation of trichloroethylene in water using BiOBr promoted by sulfite addition

Bahngmi Jung[1*], Wei Deng[2], Ying Li[2], Bill Batchelor[3] and Ahmed Abdel-Wahab[1,3*]

## Abstract

**Background:** Photodegradation of trichloroethylene (TCE) in aqueous solution under simulated solar light irradiation was studied under different experimental conditions to determine the reaction mechanism and kinetics that control TCE degradation using bismuth oxybromide (BiOBr) in the presence of sulfite. Photocatalysts were synthesized to be more responsive to visible light under simulated solar light and particular attention was focused on the reactive specie formed by reaction of the sulfite on the surface of BiOBr under simulated sunlight.

**Result:** Degradation rate of TCE was greatly enhanced by the presence of sulfite, and the enhancement increased with sulfite dose to a maximum that was retained at higher sulfite doses. Degradation rate of TCE was also affected by other factors, such as initial TCE concentration, BiOBr dose, and solution pH. In addition, the cycling performance of BiOBr was examined, and the amount of TCE degraded was almost constant over increasing cycle numbers when initial sulfite concentration was high enough to maintain a suitable sulfite concentration throughout the experiment. When TCE was degraded by BiOBr in the presence of sulfite under simulated sunlight irradiation, the major by-product measured was the non-hazardous chloride ion, and dechlorination efficiency was about 58%.

**Conclusion:** This study extended the use of a potential effective photocatalyst (BiOBr) to a semi-volatile organic contaminant (TCE), not limited to mainly focus on organic dyes, and evaluated the use of sulfite as a hole scavenger in order to enhance the degradation of TCE without needing to manipulate the structure of BiOBr. The active species being responsible for TCE degradation in BiOBr/TCE/sulfite system under simulated solar light was the sulfite radical ($SO_3^{\cdot-}$), and the photocatalytic activity of BiOBr did not decrease over a number of treatment cycles when $S_{IV}$ dose was sufficient.

**Keywords:** Trichloroethylene, Photocatalytic degradation, BiOBr, Sulfite, Solar light

## Background

Trichloroethylene (TCE) has been used as a solvent in industrial processes, such as an intermediate in the refrigerant manufacturing, as a degreasing solvent, and as a spotting agent for dry cleaning [1]. It is estimated that around 250 million pounds per year are produced in or imported into the United States [2]. TCE is the most common pollutant in groundwater in the United States due to the leaks from underground storage tanks and improper disposal [3]. Exposure to high levels of TCE can cause nervous system effects, liver and lung damage, irregular heartbeat, unconsciousness, and possibly death. The maximum contaminant level (MCL) for TCE set by United States Environmental Protection Agency (USEPA) is 5 µg/L and its concentration in discharged wastewater should not exceed 54 µg/L [4]. Many TCE removal techniques have been reported in the literature. These treatment processes include bioremediation,

*Correspondence: bahngmi.jung@qatar.tamu.edu; jung.bahngmi@gmail.com; ahmed.wahab@qatar.tamu.edu
[1] Chemical Engineering Program, Texas A&M University at Qatar, Education City, P.O. Box 23874, Doha, Qatar
Full list of author information is available at the end of the article

thermal treatment, chemical oxidation, and electrokinetic remediation [5–8]. Conventional treatment technologies can be effective in removing TCE from polluted waters, but in these cases it is often transferred from one phase to another without being destroyed. Application of advanced oxidation processes (AOPs) is an alternative approach to destroying recalcitrant organic compounds. Typical AOP combinations include $UV/O_3$, $UV/H_2O_2$, and $UV/O_3/H_2O_2$ with and without photocatalysts [9–14]. The final products of TCE degradation by AOPs include chloride, formic acid, dichloroacetic acid, monochloroacetic acid, glyoxylic acid, monochloroacetylene, dichloroacetylene, formaldehyde, dichloroacetaldehyde, and oxalic acid. The $TiO_2$-mediated photocatalytic degradation of TCE has been investigated by many researchers and their results are summarized in Additional file 1: Table S1. Pruden and Ollis [15] reported complete mineralization to HCl and $CO_2$ of TCE in aqueous solution using illuminated titanium dioxide, and identified dichloroacetaldehyde as an intermediate. Phillips and Raupp [16] suggested that hydroxyl radical or hydroperoxide radical initialized the photocatalytic reaction of TCE and measured dichloroacetaldehyde an intermediate. Glaze et al. [17] have proposed two pathways for TCE photodegradation; a reductive pathway involving conduction band electrons and an oxidative pathway leading to mineralization. They found dichloroacetaldehyde (DCAAD), dichloroacetic acid (DCAA), and trichloroacetic acid (TCAA) as products. Yamazaki-Nishida et al. [3] proposed a mechanism including an initial reaction with hydroxyl radicals and monochloroacetate as an intermediate. Fan and Yates [2] have investigated the photooxidation of TCE on $TiO_2$ using infrared spectroscopy and the intermediate they identified was dichloroacetyl chloride ($HCl_2CCOCl$).

Semiconductor photocatalysts containing $TiO_2$ hold great promise as an effective and green technologies for addressing energy generation and environmental purification on a global scale. However, $TiO_2$ can only respond to ultraviolet (UV) light, which accounts for only about 4% of the solar spectrum. Its limited absorption of visible light results from the rapid recombination of electron–hole pairs and the wide band gap of $TiO_2$ (e.g., 3.2 eV for anatase). To overcome this limitation, a number of strategies have been applied to modify $TiO_2$, including doping [18, 19], sensitization [20, 21], forming heterostructures [22], and coupling with π-conjugated architectures [23]. Also, many researchers have explored novel visible-light-active photocatalysts such as bismuth oxyhalides (BiOXs, X=F, Cl, Br, I) [24–29]. Bismuth-based materials could be appropriate candidates owing to the fact that Bi 6s in Bi(III) hybridize O 2p levels to push up the position of the valence band (VB), thus narrowing the band gap to harvest visible light [24]. Published data for the photoactivity of bismuth oxyhalides under visible light [30–33] are summarized in Additional file 1: Table S2, which includes our previous study for degradation of methyl orange (MO) [34]. Bismuth oxyhalides is very promising as an improved visible light-driven photocatalyst for TCE degradation. Among BiOXs, BiOBr has a tetragonal matlockite (PbFCl) structure characterized by $[Bi_2O_2]$ slabs interleaved with double Br atom slabs with an internal electric field perpendicular to each layer, which is beneficial for the generation and separation of photogenerated electron–hole pairs [35]. BiOBr has been extensively studied due to its unique properties and potential applications for environmental remediation. However, its application has been limited to a few contaminants, mainly focused on organic dyes such as MO and Rhodamine B (RhB).

This study extends the use of a potential effective photocatalyst (BiOBr) to a semi-volatile organic contaminant (trichloroethylene or TCE), and evaluates the use of sulfite as a hole scavenger in order to enhance the degradation of TCE without needing to manipulate the structure of BiOBr. When the sulfite ion is added to a solution, acid–base reactions can form bisulfite ($HSO_3^-$) and sulfurous acid ($H_2SO_3$). The total concentration of these species will be identified as $S_{IV}$. The sulfite radical is produced by reaction of $S_{IV}$ with a hole or an aqueous hydroxide radical and is an active specie that can react both as an oxidant and a reductant. It can be applied to effectively degrade organics such as phenol, chlorpromazine, olefins, and polyunsaturated fatty acids [36–39]. Previous studies showed that sulfite radical formed by UV irradiation of $S_{IV}$ was effective in degrading trichloroethylene [40], and vinyl chloride [41].

In summary, the objectives of this study were to (1) evaluate the effectiveness of photocatalytic degradation of TCE using BiOBr with addition of sodium sulfite ($Na_2SO_3$) under simulated solar light; (2) examine the effects of the process variables such as $S_{IV}$ dose, photocatalyst dose, pH, and initial TCE concentration; (3) assess the cycling performance of the photocatalyst (BiOBr) by repeating the photodegradation experiment; and (4) study the photocatalytic reaction mechanism for TCE photocatalytic degradation by BiOBr with $S_{IV}$ addition.

## Materials and methods

### Materials

Bismuth nitrate pentahydrate ($Bi(NO_3)_3{\cdot}5H_2O, \geq 98.0\%$), commercial $TiO_2$ nanopowders, (P25), hexane (95%), sodium chloride ($\geq 99.5\%$) were obtained from Sigma-Aldrich and potassium bromide (KBr) was obtained from Beantown Chemical Inc. (New Hampshire, US). Sodium

sulfite anhydrous ($Na_2SO_3$, 98.0%) and sodium nitrate ($NaNO_3$, FCC purified) were purchased from Mallinckrodt Chemicals. The chemical used as a target organic compound was trichloroethylene (≥ 99.5%, ACS reagent, Sigma-Aldrich). All aqueous solutions were prepared using deionized deoxygenated water (DDW) in anaerobic chamber (Coy Laboratory Products) that was filled with nitrogen gas (99.99%). DDW was prepared by deoxygenating 18 MΩ-cm deionized water with 99.99% nitrogen for 2 h and then stored in anaerobic chamber. Stock solutions of chlorinated organic was prepared daily by diluting them in methanol (99+%, HPLC grade, Fisher Scientific). TCE stock and standard solutions were prepared in glass vials (nominally 20 mL) and closed using butyl rubber septa and aluminum caps. A volume of 10 µL of a methanolic stock solution of TCE was spiked using a gas-tight syringe into a batch reactor (41.6 ± 0.1 mL, nominally 40 mL, a quartz vial) containing photocatalysts and $S_{IV}$. The reactor was filled in a way that eliminated headspace, but some headspace formed after sampling. The standard concentration of a target organic, TCE was desired to be 0.25 mM in a reactor. To confirm the effectiveness of solar light-driven advanced reduction process (SARP) using BiOBr and $S_{IV}$, batch experiments at six different conditions were first conducted as controls. The controls are as follows: (1) TCE + water + no light, (2) TCE + water + light, (3) TCE + $S_{IV}$ + no light, (4) TCE + $S_{IV}$ + light, (5) TCE + BiOBr + no light, and (6) TCE + BiOBr + light. From the results of controls at six different conditions, TCE loss due to sorption (reactor wall, septa) or volatilization will be evaluated and TCE degradation with the addition of $S_{IV}$ alone under simulated solar light without photocatalyst will be estimated.

#### Analytical methods

To measure TCE concentration, a 10-µL aqueous sample was rapidly transferred using a gas-tight syringe into a GC amber vial (nominally 2 mL) containing 1 mL hexane. After shaking at 250 rpm for 30 min, the GC vial was transferred into a GC autosampler. TCE was analyzed using an Agilent Technologies 7890A gas chromatograph (GC) equipped with a micro-electron capture detector (µECD) with a DB-1 column (Agilent Technologies J&W 123-1035, length 30 m, I.D. 0.320 mm, and film thickness 5.0 µm). The amount of each injected samples was 0.1 µL with a split ratio of 10:1. The oven temperature program began at 40 °C, which was held for 5 min, was increased at 10 °C/min to 150 °C, was held for 3 min, was increased at 25 °C/min to 230 °C and was held for 2 min. The temperatures of the injector and detector were 210 °C and 280 °C, respectively. Helium was used as a carrier gas with a flow rate of 45 mL/min and nitrogen was used as a makeup gas with a flow rate of 20 mL/min. A Dionex IC 2000 ion chromatograph was used to measure concentrations of chloride and sulfite ions. Carbon dioxide was measured by a GC with a thermal conductivity detector (GC/TCD). Surface morphology of photocatalyst was characterized before or after irradiation using a scanning emission microscope (SEM) (Quanta 400 SEM, FEI, Inc.)

#### Preparation of BiOBr

For the synthesis of bismuth oxybromide (BiOBr), 0.98 g bismuth (III) nitrate pentahydrate and 0.729 g hexadecyltrimethylammonium bromide were dissolved in 30 mL ethylene glycol. The solution was then put into a 50 mL Teflon-lined autoclave and heated at 160 °C for 12 h. The obtained product from the autoclave was washed with water and dried. Surface characterization of BiOBr sample that can absorb light in the visible region and its photocatalytic activity for degrading methyl orange were confirmed in our previous studies [34, 42] and some results were summarized in this work. The X-ray power diffraction (XRD) pattern of BiOBr sample indicated high crystallinity with diffraction peaks indexed to the tetragonal structure of BiOBr (JCPDS File No. 73-2061) [42]. The major diffraction peaks located near to $2\theta = 32^{\circ}$ were deconvoluted to two peaks, which matched to (012) and (110) facets of BiOBr phase. Scanning electron microscope (SEM) images showed that BiOBr had a three dimensional hierarchical microspherical structure (see Additional file 1: Fig. S1). The microspheres were made of densely stacked thin microplates formed from the layered structure of the bismuth oxyhalide, and interconnected to form larger aggregates. In addition, the Brunauer–Emmett–Teller (BET) surface area of the BiOBr sample was measured to be 22 $m^2/g$. The light absorption of pure BiOBr was located in the UV range and the calculated conduction band and valence band positions were 0.27 V and 3.09 V vs. NHE, respectively. X-ray photoelectron spectroscopy (xps) was used to study the surface compositions and chemical states of BiOBr samples and the survey spectra showed the presence of Bi, O, Br and C in BiOBr samples. It was reported that the Bi 4f spectra of BiOBr can be split into two parts where the binding energies are located at 159.4 eV and 164.8 eV that correspond to Bi $4f_{7/2}$ and Bi $4f_{5/2}$, respectively, and it indicates the existence of $Bi^{3+}$ of the BiOBr samples [42].

#### Photocatalytic degradation experiments

A solar light-driven advanced reduction process (SARP) was evaluated by studying the abilities of various photocatalysts with or without $S_{IV}$ to degrade TCE in anaerobic condition. The solution containing photocatalyst was prepared in DDW and mixed for 1 h before being transferred into a 40 mL-quartz vial. The standard dose of photocatalyst in a reactor was 1 g/L. 10 µL of TCE stock

solution was added into a reactor to yield a concentration of 0.25 mM. Prior to irradiation, the reactor solution containing TCE and photocatalyst with or without $S_{IV}$ was magnetically stirred in the dark for 1 h to ensure adsorption/desorption equilibrium. The simulated solar light source was purchased from Abet Technologies (model 11002 Sunlite) and included a 100 W Xr arc lamp/reflector. The distance and orientation between light source and reactor was kept constant in all batch experiments, and one quartz reactor was used in all batch tests.

Batch kinetic tests were conducted for TCE degradation using photocatalysts (titanium-doped bismuth oxyhalides, Ti–BiOX, X=Cl, Br and pure bismuth oxyhalides), but the photocatalyst alone was not effective in degrading TCE. The effectiveness of four different photocatalysts (BiOBr, Ti–BiOBr, BiOCl, and Ti–BiOCl) with and without addition of $S_{IV}$ was investigated in preliminary experiments (see Additional file 1: Fig. S2). As shown in Additional file 1: Fig. S2, the photocatalyst, BiOBr with the addition of $S_{IV}$ showed the greatest TCE removal (78%).

The effect of pH on TCE degradation was studied in a series of batch experiments in which a solution containing BiOBr and $S_{IV}$ was prepared in a glass beaker and the desired initial pH ($pH_0$) was obtained by adding 6 N HCl or 1 N NaOH. The solution was transferred into a quartz vial right after reaching to a desired pH and the vial was capped before the TCE stock solution was injected using a gas-tight syringe. Experimental conditions of batch tests are shown in Additional file 1: Table S3.

## Results and discussion

Figure 1 shows TCE concentrations in controls with open symbols indicating the absence of solar light and closed symbols indicating its presence. The presence or absence of solar irradiation had little effect on loss of TCE, which indicates that the process was not photoactive. Although the initial TCE concentrations changed a little, the slopes were similar whether $S_{IV}$ or BiOBr were present. The lack of effect of these variables indicates that the small losses of TCE were due to physical processes such as sorption or volatilization. Figure 2 compares the photocatalytic ability of $TiO_2$ (P25) and pure BiOBr for TCE degradation with addition of $S_{IV}$ under simulated solar light. The degradation efficiency ($(1 - C_f/C_0)$ * 100 (%)) for BiOBr reached 78% after 210 min irradiation, whereas it reached 15% after 240 min for P25. Pseudo-first-order rate constants were calculated as 0.008 ($min^{-1}$) and 0.0007 ($min^{-1}$) for BiOBr and P25, respectively.

Our previous studies have proven that sulfite radical is an effective specie for TCE degradation [40]. Sulfite radicals are usually created upon the photolysis of $S_{IV}$ under middle UV light. Sulfite radical exhibits

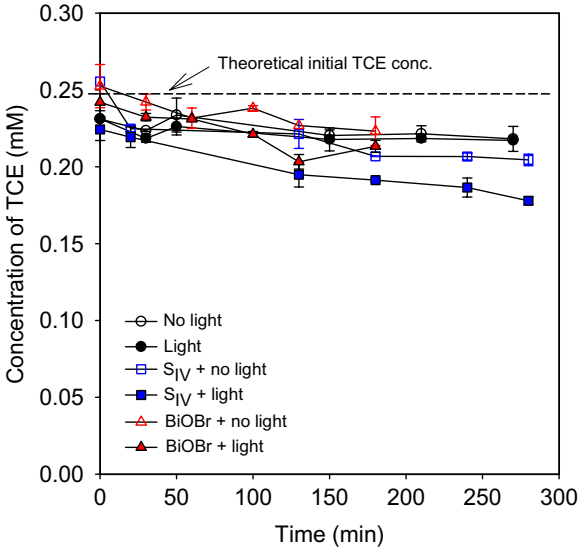


**Fig. 1** TCE concentrations in controls. Conditions: $[TCE]_0 = \sim 0.25$ mM, $[SO_3^{2-}]_0 = 25$ mM, BiOBr = 1 g/L, and the solution pH was not buffered

an optical absorption centered at 250 nm, $\varepsilon = 1380$ $Lmol^{-1}cm^{-1}$ and its absorption spectrum tail extends to 400 nm [43, 44]. The sulfite radical formation could occur in different ways: (1) $S_{IV}$ could directly absorb solar light and produce the radical by direct photolysis ($SO_3^{2-} + h\nu \rightarrow SO_3^{\cdot-} + e_{aq}^-$) or (2) sulfite radical could be formed by the reaction of $S_{IV}$ with the hydroxyl radical that is produced in the valence band of BiOBr ($SO_3^{2-} + {}^{\cdot}OH_{VB} \rightarrow SO_3^{\cdot-} + OH^-$), or (3) sulfite radical could be formed by direct reaction with photoinduced holes ($SO_3^{2-} + h_{VB}^+ \rightarrow SO_3^{\cdot-}$). However, results in Fig. 1 indicate that little degradation occurs in $S_{IV}$ solutions irradiated by simulated solar light, so production of radicals by direct photolysis of $S_{IV}$ is unlikely. Pure P25 has a wide band gap, so it will not absorb much visible light, which will result in production of few hydroxyl radicals, leading to low levels of TCE oxidation. The band gap (3.2 eV) of $TiO_2$ means that its excellent photocatalytic activities are only achieved when illuminated by ultraviolet light. It is known that solar light includes 4% of UV light [45] so that $TiO_2$ can absorb some UV photons when irradiated with solar light. The decrease of TCE concentration observed with P25 in Fig. 2 could be attributed to photocatalysis associated with absorption of UV photons in simulated solar light spectrum, but it could also be due to sorption onto P25 particles. Although BiOBr has a narrow band gap (~2.82–2.87 eV) and absorb visible light [46], BiOBr did not result in effective TCE degradation without $S_{IV}$ (Fig. 1). As shown in Fig. 2, when $S_{IV}$ was

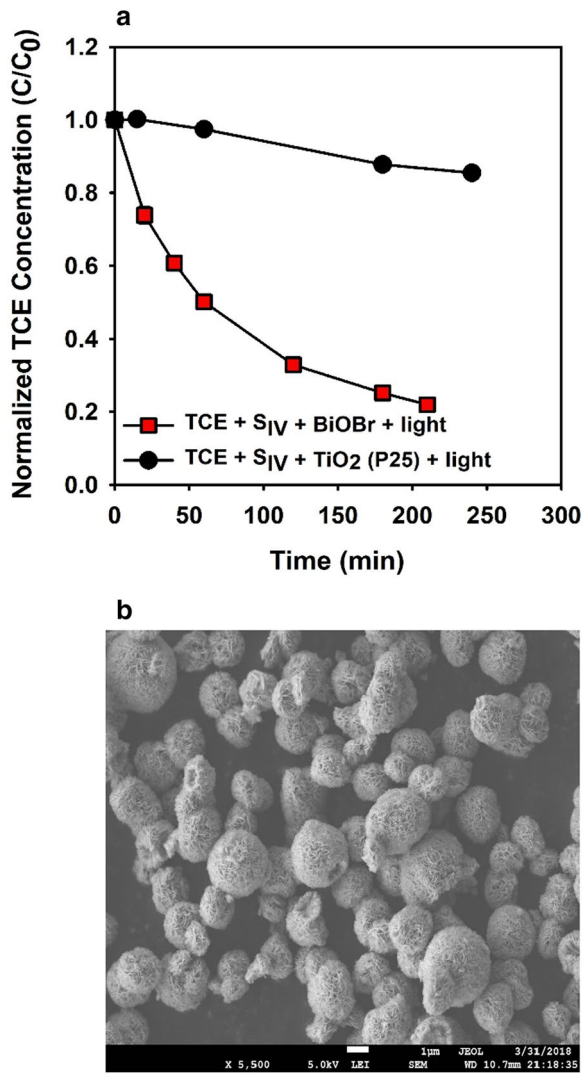


**Fig. 2** Comparison of photocatalytic activity of $TiO_2$ (P25) and BiOBr to degrade TCE with addition of $S_{IV}$ under simulated solar light (**a**) and SEM image of pure BiOBr (**b**). Conditions: $[TCE]_0 = \sim 0.25$ mM, $[SO_3^{2-}]_0 = 25$ mM, BiOBr or $TiO_2 = 1$ g/L, and the solution pH was not buffered

added to the system of BiOBr/TCE (photocatalyst/contaminant) with simulated sunlight irradiation, TCE was effectively degraded.

### Effect of sulfite dose

First, the effect of $S_{IV}$ dose on TCE degradation in the system of BiOBr/TCE under simulated solar light was investigated (Fig. 3a). In all experiments, initial TCE concentration and BiOBr dose were 0.25 mM and 1 g/L, respectively. $S_{IV}$ dose was varied from 0 to 50 mM. When $S_{IV}$ dose was increased from zero to 1.25 mM the percentage of TCE removal increased rapidly, but above 1.25 mM the removal was constant (Fig. 3b). Therefore, it appears that a $S_{IV}$/TCE molar ratio around 5 is required to provide sufficient $S_{IV}$ to degrade TCE. Here, the percentage of TCE removal was calculated by Eq. (1):

$$\text{Removal efficiency} = \left(C_0 - C_{t,\text{final}}\right)/C_0 \times 100\,(\%), \quad (1)$$

where $C_0$ (mM) and $C_{t,\text{final}}$ (mM) present the TCE concentration at $t = 0$ and $t = t_{\text{final}}$, respectively.

In addition, the pseudo-first-order rate constants were calculated using TCE concentrations and a first-order decay model ($-\text{Ln}(C_t/C_0) = kt$), where $C_0$ (mM) and $C_t$ (mM) represent the TCE concentration at $t = 0$ and any time, $t$, and $k$ is the rate constant. The rate constants were determined to be 0.0011, 0.0043, 0.0187, 0.0151, 0.0178, and 0.0257 ($\text{min}^{-1}$) with increasing $S_{IV}$ doses. At low $S_{IV}$ doses, the rate constant very rapidly increased till $S_{IV}$ dose is 1.25 mM, but at higher sulfite doses its increase was reduced.

At higher $S_{IV}$ concentration constant TCE removal efficiency could be due to light absorption of by-products from $S_{IV}$ degradation. As they accumulate, there will be less light available at the surface of the photocatalyst to produce active species for TCE reduction. Absorbance of $S_{IV}$ solutions varies with pH and concentration with absorbance increasing at wavelengths below 250 nm [47, 48]. UV–vis absorption spectra of different solutions containing TCE, BiOBr and $S_{IV}$ were measured (Fig. 4). Although measurement of absorbance at high $S_{IV}$ dose is unreliable, higher $S_{IV}$ concentration (10 mM vs. 2 mM) absorbed more light in the range between 230 and 250 nm, and a noticeable peak occurred after a period of irradiation. Additionally, absorbance of $S_{IV}$ was characterized at different $S_{IV}$ doses and irradiation times in experiments on MO degradation (Additional file 1: Fig. S3). For a mixture of MO and $TiO_2$ with simulated solar light irradiation, a peak was observed at 243 nm that not found in solutions of MO alone and its magnitude increased with irradiation time. The MO peak at 464 nm decreased with irradiation time, indicating that MO was being transformed into a product that absorbs at 243 nm. This supports our hypothesis that higher $S_{IV}$ doses lead to higher concentrations of products that absorb more light. These products may adsorb on the surface of the photocatalyst and affect surface chemistry, possibly by limiting the production of photoinduced electrons and holes.

Figure 3c shows the relationship between initial degradation rates and $S_{IV}$ doses. Initial rates ($r_0$) were calculated as the product of the first-order rate constant and initial concentration, using TCE concentrations up to 60 min. The fitted model equation in Fig. 3c was $r_0 = ax/(b + x)$, where $x$ is $S_{IV}$ dose (mM) and calculated parameters were $a = 0.0055$ (mM/min) and $b = 0.42$ (mM).

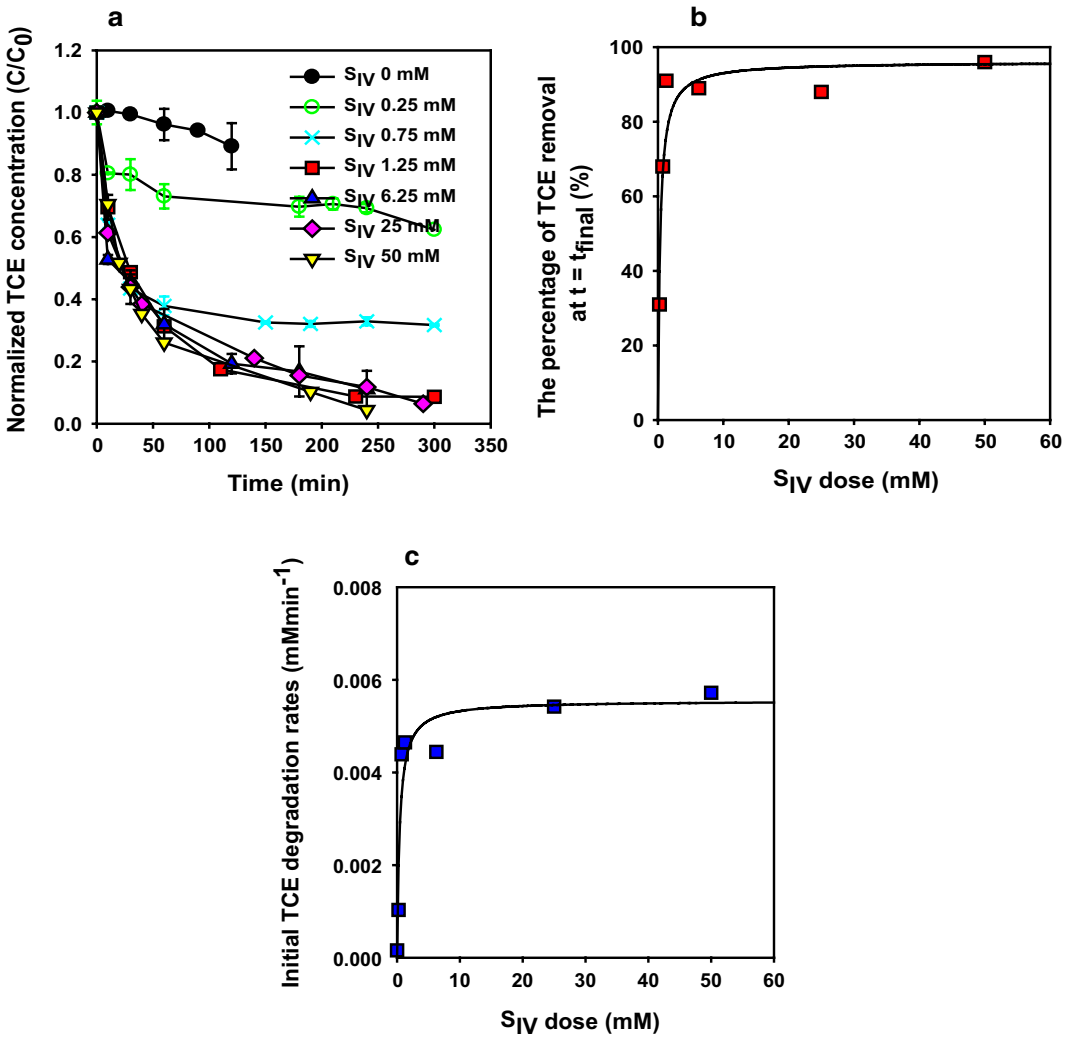


**Fig. 3** Effect of $S_{IV}$ dose on TCE degradation in BiOBr/TCE/$S_{IV}$ (photocatalyst/contaminant/reagent) system under simulated sunlight (**a**), the relationship between $S_{IV}$ dose and the percentage of TCE removal at $t = t_{final}$ (**b**), and the relationship between $S_{IV}$ dose and initial degradation rates ($r_0$) (**c**). Conditions: $[TCE]_0 = \sim 0.25$ mM, BiOBr dose = 1 g/L, and no pH control. The fitted model equation in **c** is $r_0 = a * x/(b + x)$, where x is $S_{IV}$ dose (mM), $a = 0.0055$ (mM/min) and $b = 0.42$ (mM)

Initial degradation rates increased rapidly at very low $S_{IV}$ dose, but became constant at higher doses. This confirms that $S_{IV}$ dose does not have an appreciable effect when it is above some minimum value. However, when the $S_{IV}$ concentration is low enough, it can control rates of TCE degradation. The results shown in Fig. 3 confirm that $S_{IV}$ is required to form the reactive specie that is involved in the photocatalytic degradation of TCE.

#### Effect of BiOBr dose

The effect of BiOBr dose on TCE degradation in the system of BiOBr/TCE with sulfite under solar light is shown in Fig. 5a. BiOBr dose was varied at 0.5 g/L, 1 g/L, and 2 g/L, while sulfite dose was constant at 25 mM. Figure 5 shows rapid initial decreases in TCE concentration, which is consistent with other reports for TCE degradation by BiOBr or BiOI [45, 49]. Zhang et al. have studied TCE degradation using nanofibers of bismuth oxyhalides, and found that TCE concentration rapidly decreased within the first 15 min of irradiation and eventually TCE concentration decreased by 31.3% in 90 min for pure BiOBr [45]. TCE removal rate gradually decreased with increasing irradiation time (Fig. 5), which is similar to that reported by Zhang et al. TCE removal rate increased with increasing BiOBr dose. When the first-order rate model was applied to the experiments shown in Fig. 5a,

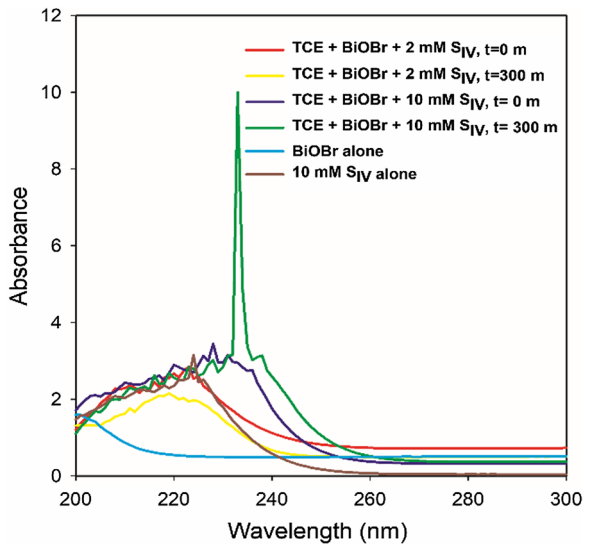


**Fig. 4** UV–Vis absorption spectra of solution under simulated solar light. Conditions: $[TCE]_0 = 0.245$ mM, BiOBr dose = 1 g/L, $S_{IV}$ dose = 2 mM or 10 mM

estimated rate constants were 0.006, 0.018, and 0.036 ($min^{-1}$) with increasing BiOBr dose (Fig. 5b).

#### Effect of initial TCE concentration

Figure 6a shows the effect of initial TCE concentration on TCE degradation. Initial TCE concentrations ranged from 0.05 to 0.5 mM, while the molar ratio of $S_{IV}$ dose to initial TCE concentration and BiOBr dose were fixed at 40, and 1 g/L, respectively. A molar ratio of 40 is equivalent to an initial $S_{IV}$ concentration of 10 mM, which is shown in Fig. 3 to provide sufficient $S_{IV}$ to degrade TCE. As initial TCE concentration increases from 0.05 to 0.25 mM the first-order rate constant, $k_{obs}$ very rapidly decreased from 0.0815 ($min^{-1}$) to 0.009 ($min^{-1}$) (Fig. 6b), and TCE concentrations were not detectable in 180 min at $[TCE]_0 = 0.05$ mM and 0.1 mM. As initial TCE concentration increases from 0.25 to 0.5 mM, $k_{obs}$ increased a little by 1.4 times (Fig. 6b). This indicates that at higher TCE concentrations a first-order model adequately describes degradation kinetics, since the rate coefficients are constant. The higher rate coefficients at lower TCE concentrations may be caused by non-degradative TCE losses as shown in Fig. 1.

The rate of TCE degradation appears to slow at longer times with $C_0 = 0.25$ mM or 0.5 mM. Since a $S_{IV}$/TCE molar ratio of 5 should be sufficient to degrade TCE as shown in Fig. 3, such behavior would not be expected. However, it could be the result of production of more by-products of $S_{IV}$ degradation that hinder TCE photodegradation by limiting the production of photoinduced electrons and holes by absorbing light or by other means.

#### Effect of pH

The solution pH in a system with 1 g/L BiOBr and 10 mM $S_{IV}$ ranged between 8.5 and 8.7 without pH control. As shown in Fig. 7, TCE degradation rate did not show any noticeable trend with solution pH. At five different initial pH values (2.98, 5.45, 7.3, 10.46, and 8.6) TCE degradation rate was the greatest at pH 5.45. At pH 8.6 TCE removal percentage at $t = 180$ min and first-order rate constant were the

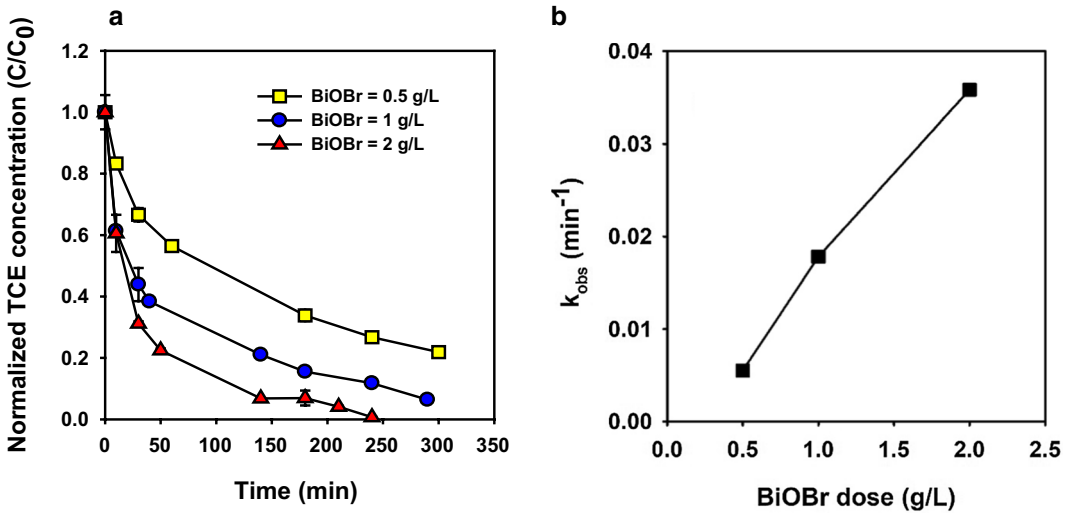


**Fig. 5** Effect of photocatalyst (BiOBr) dose on TCE degradation in BiOBr/TCE/$S_{IV}$ system under simulated sunlight (**a**) and the pseudo-first-order rate constant dependent on the BiOBr dose (**b**). Conditions: $[TCE]_0 = \sim 0.25$ mM, $[SO_3^{2-}]_0 = 25$ mM, and the solution pH was not buffered

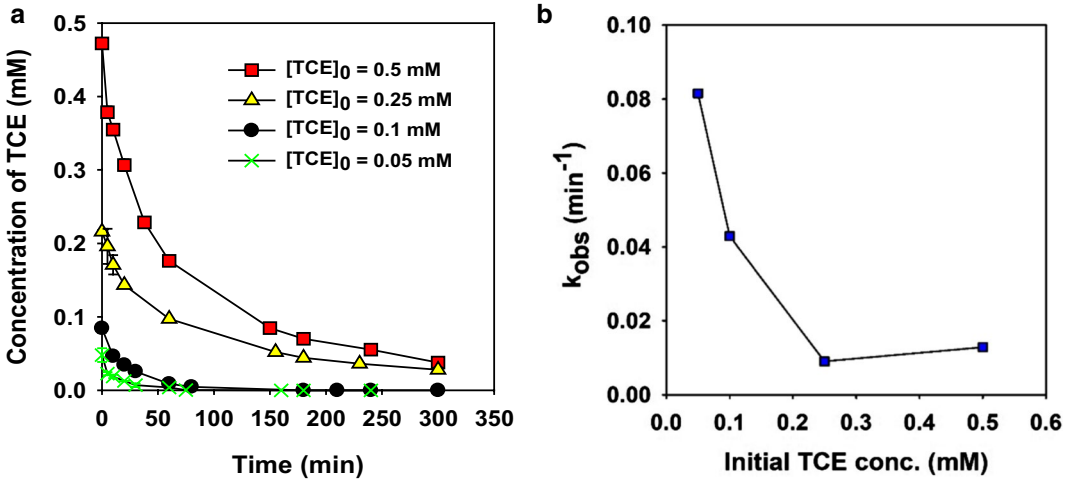


**Fig. 6** Effect of initial TCE concentration on the TCE degradation in BiOBr/TCE/$S_{IV}$ system under simulated sunlight (**a**) and the pseudo-first-order rate constant dependent on initial TCE concentrations (**b**). Conditions: the molar ratio of initial $S_{IV}$ concentration to the initial TCE concentration was fixed at 40, BiOBr = 1 g/L, and no pH control

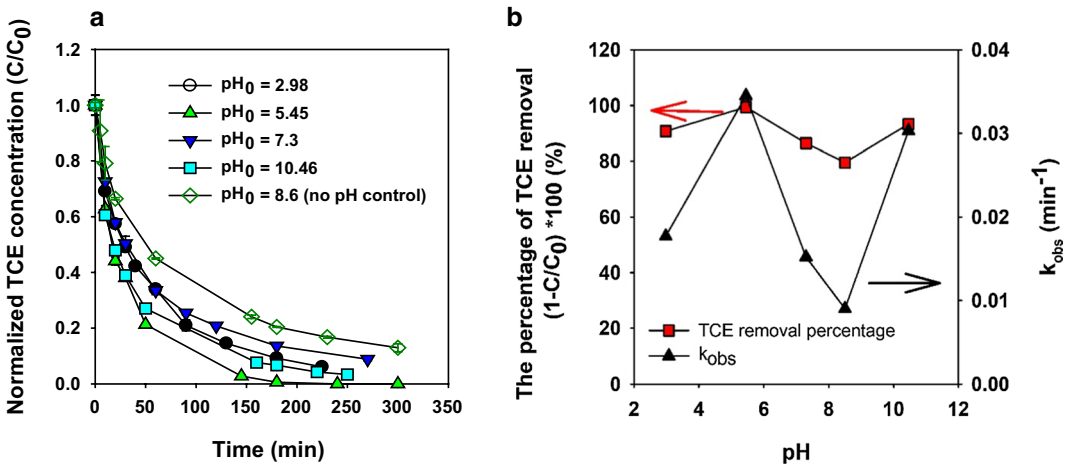


**Fig. 7** Effect of pH on TCE degradation in BiOBr/TCE/$S_{IV}$ system under simulated sunlight (**a**) and the percentage of TCE removal at $t = 180$ min and the pseudo-first-order rate constant dependent on initial solution pH ($pH_0$) (**b**). Conditions: $[TCE]_0 = \sim 0.25$ mM, $[SO_3^{2-}]_0 = 10$ mM, BiOBr = 1 g/L, and the solution pH was controlled by 6 N HCl or 1 N NaOH

smallest among experiments at five different pH values. Estimated pseudo-first-order rate constants were 0.018, 0.035, 0.015, 0.009, and 0.030 ($min^{-1}$) with increasing $pH_0$ values (2.98, 5.45, 7.3, 8.6, and 10.46) (Fig. 7b). The solution pH was generally lower at the end of the experiment compared to the start of the experiment (see Additional file 1: Fig. S7), but the magnitude of change was not great. It has been reported that pH decreases during TCE degradation by a similar photocatalyst (BiOCl) under UV light and this was explained by $H^+$ generation during TCE degradation. In our study, at $pH_0 = 5.45$ the solution pH decreased to 2.82 in 300 min. The concentrations of species produced from $S_{IV}$ by acid–base reactions ($SO_3^{2-}$, $HSO_3^-$, and $H_2SO_3$) will change with pH. At weakly acidic pH ($\sim pH_0 = 5.45$), $HSO_3^-$ will be the dominant specie. The greatest TCE degradation found at $pH_0 = 5.45$, which indicates that bisulfite ion also participates to form active radicals.

$$HSO_3^- + h_{vB}^+ \rightarrow SO_3^{\cdot -} + H^+ \quad (2)$$

This might explain why the greatest change in pH was observed in the experiment with the greatest TCE removal.

### Cycling performance to degrade TCE

Cycling performance was evaluated through batch kinetic experiments. When BiOBr dose was 1 g/L and $S_{IV}$ dose was 2 mM or 10 mM, TCE concentrations rapidly decreased at the beginning of the experiment and removals reached 72–73% after 90 min in the 1st cycle (Fig. 8). At the beginning of each cycle, 10 µL of the same TCE stock solution used in the first cycle was injected to the reactor. This increases the TCE concentration by approximately 0.25 mM. Initial TCE concentrations ($C_0$) for each cycle were calculated by adding 0.25 mM to the final concentration measured in the previous cycle. When $S_{IV}$ dose was 2 mM, the amount TCE degraded was 0.0070, 0.0058, and 0.0045 mmol for the 1st, 2nd, and 3rd cycle, respectively (Fig. 8a). When $S_{IV}$ dose was 10 mM, the amount of TCE degraded was 0.0068, 0.0079, and 0.0065 mmol at each cycle (Fig. 8b). As shown in Fig. 3, TCE degradation was almost the same at if $S_{IV}$ doses was greater than or equal to 1.25 mM. As shown in Fig. 8a, b, TCE degradation was similar during the 1st cycle, regardless of $S_{IV}$ dose, because there was sufficient $S_{IV}$ dose to degrade the amount of TCE present initially. However, at the lower $S_{IV}$ dose (2 mM), the amount of TCE degraded decreased at 2nd and 3rd cycle (Fig. 8a). Whereas at the higher $S_{IV}$ dose (10 mM), the amount of TCE degraded TCE increased a little or was constant (Fig. 8b).

Figure 9 shows TCE degradation only when TCE is injected at the start of a cycle (Fig. 9a) and when $S_{IV}$ and TCE are injected together (Fig. 9b). Initial concentrations of TCE and $S_{IV}$ for the first cycle were 0.1 mM and 4.0 mM ($S_{IV}$/TCE = 40). When $S_{IV}$ was not added at the start of the cycle, the $S_{IV}$/TCE molar ratio would be 20 and 13.3 for the second and third cycles, respectively.

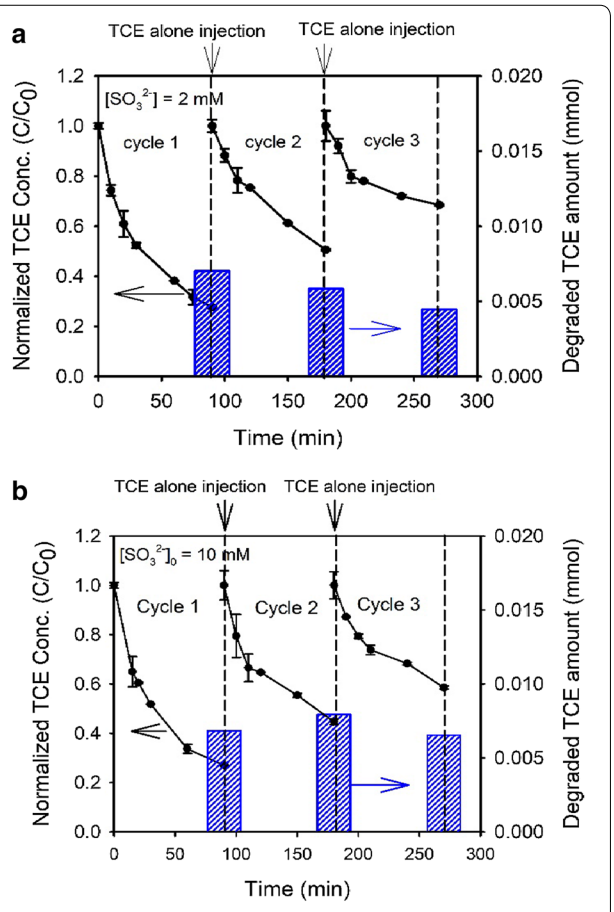


**Fig. 8** Effect of $S_{IV}$ dose on cycling performance of BiOBr in degrading TCE in the presence of $S_{IV}$ under simulated sunlight. Conditions: **a** $S_{IV}$ dose = 2 mM, **b** $S_{IV}$ dose = 10 mM, $[TCE]_0$ = ~ 0.25 mM, BiOBr = 1 g/L, and the amount of TCE injected at each cycle increased TCE concentration by ~ 0.25 mM. In all experiments, the solution pH was not controlled

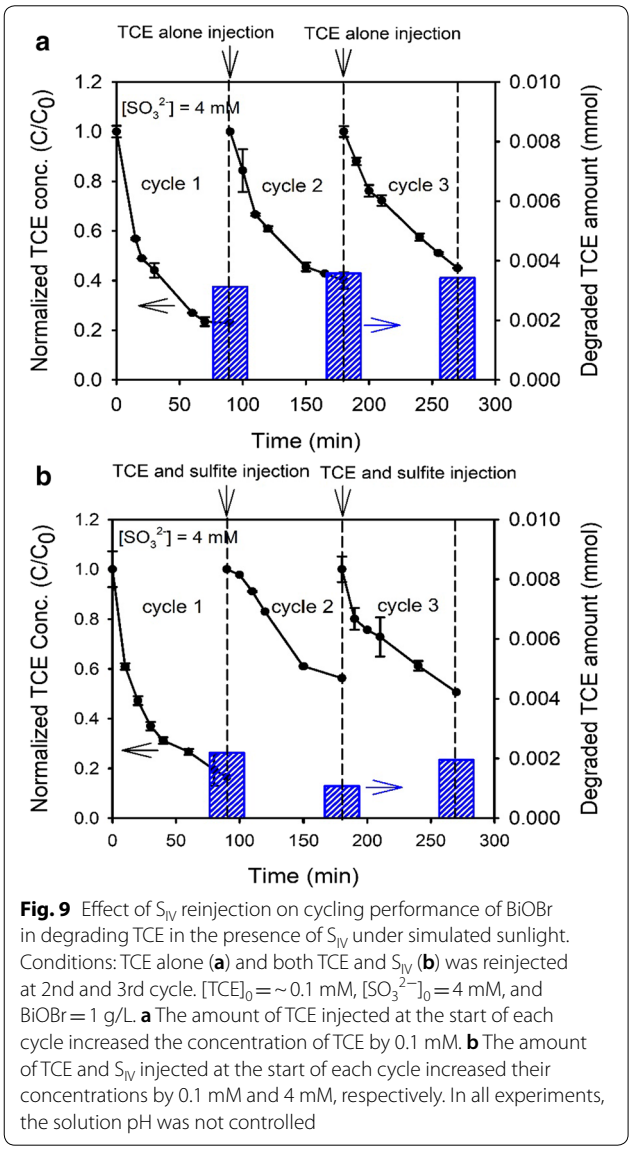


**Fig. 9** Effect of $S_{IV}$ reinjection on cycling performance of BiOBr in degrading TCE in the presence of $S_{IV}$ under simulated sunlight. Conditions: TCE alone (**a**) and both TCE and $S_{IV}$ (**b**) was reinjected at 2nd and 3rd cycle. $[TCE]_0$ = ~ 0.1 mM, $[SO_3^{2-}]_0$ = 4 mM, and BiOBr = 1 g/L. **a** The amount of TCE injected at the start of each cycle increased the concentration of TCE by 0.1 mM. **b** The amount of TCE and $S_{IV}$ injected at the start of each cycle increased their concentrations by 0.1 mM and 4 mM, respectively. In all experiments, the solution pH was not controlled

Therefore, the $S_{IV}$/TCE ratio was well above 5, which was identified previously as the minimum for complete TCE removal. This is confirmed in the results shown in Fig. 9a, where the amount of TCE degraded did not decrease with increasing cycle, which indicates that the capability of a photocatalyst, BiOBr did not decrease (Fig. 9a). When $S_{IV}$ was added at each cycle (Fig. 9b), the amount of TCE degraded did not increase, rather it decreased. As shown in Fig. 3, increasing $S_{IV}$ dose would not be expected to enhance TCE degradation rate, if it were above a $S_{IV}$/TCE ratio of 5.

Figure 10 shows the effect of initial TCE concentration on cycling performance of BiOBr. Initial TCE concentration at $t=0$ was 0.1 mM and 0.25 mM, in Fig. 10a, b, respectively. At the start of the second cycle, the same concentrations of TCE were added, resulting in higher concentrations than at $t=0$. $S_{IV}$ dose was 40 times higher than the initial molar TCE concentration in both experiments. When initial TCE concentration was 0.1 mM (Fig. 10a), the amounts of TCE degraded in 90 min were 0.0032 mmol and 0.0033 mmol, for the 1st and 2nd cycle, respectively. When initial TCE concentration was 0.25 mM (Fig. 10b), the amount of TCE degraded over 120 min in the first cycle was 0.0065 mmol, which was estimated by linear interpolation, and the amount degraded over 120 min in the second cycle was 0.0043 mmol. It seems that the capability of BiOBr to degrade TCE decreased slightly, but this could be explained by the higher TCE concentration at the start of the second cycle compared to the initial concentration for the first cycle. Additional file 1: Table S4 shows the pseudo-first-order rate constants estimated in batch tests shown in Figs. 8, 9, 10. Generally, $k_{obs}$ decreased with increasing cycle numbers. Figure 11 shows the relationship between initial TCE concentration and the first-order rate constant ($k_{obs}$) using initial TCE concentration measured at the start of each cycle ($C_{0\_cycle}$). As shown in Fig. 11, first-order TCE degradation rate coefficients generally decreased with increasing initial TCE concentration ($C_{0\_cycle}$), with the decrease being most severe at lower concentrations as observed in Fig. 6. In these experiments, a constant amount of TCE was injected at every cycle, regardless of the concentration of TCE in the reactor at the end of the previous cycle. When 2nd and 3rd cycles started, the TCE concentrations were higher than that at $t=0$ because some TCE remained at the end of the cycle. The decrease in TCE degradation rate constant (see Additional file 1: Table S4) with increasing cycle numbers was probably the result of increasing initial TCE concentrations, not the result of a decrease in the photoactivity of BiOBr.

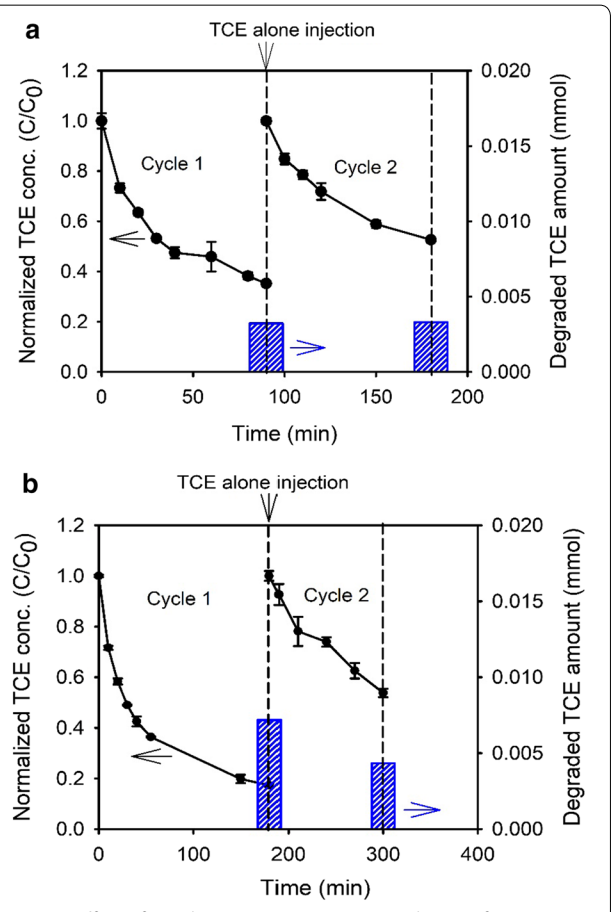


**Fig. 10** Effect of initial TCE concentration on cycling performance of BiOBr in degrading TCE in the presence of $S_{IV}$ under simulated sunlight. Conditions: BiOBr dose = 1 g/L, **a** $[TCE]_0 = \sim 0.1$ mM, $[SO_3^{2-}]_0 = 4$ mM at $t=0$ min, **b** $[TCE]_0 = \sim 0.25$ mM, $[SO_3^{2-}]_0 = 10$ mM at $t=0$ min, and the amounts of TCE and $S_{IV}$ injected increased their concentrations by 0.1 mM, and 0.25 mM, respectively

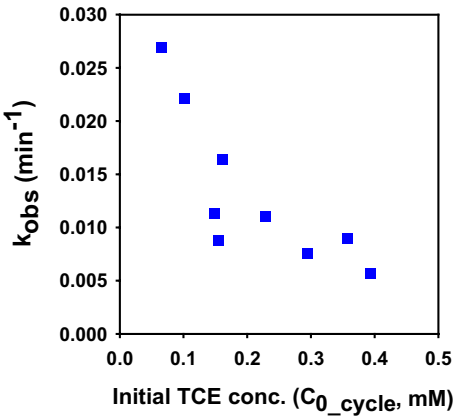


**Fig. 11** The relationship between initial TCE concentration ($C_{0\_cycle}$) and the pseudo-first-order rate constant of TCE degradation. These data were obtained from the experiments that study cycling performance of photocatalysts shown in Figs. 8, 9, 10

### Reaction mechanism

TCE degradation can be explained by three possibilities: (1) reaction with hydroxyl radicals or photoinduced holes; (2) reaction with sulfite radicals, or (3) reaction with photoinduced electrons or hydrated electrons. Under simulated solar light, electrons in the valence band (VB) of BiOBr can be excited up to a higher potential edge (~0.27 eV), leaving a photoinduced hole (Eq. (3)). The holes in the valence band of BiOBr can oxidize water or hydroxide ion to produce hydroxyl radicals (Eq. (4)) ($OH\cdot/OH^-$, +2.18 eV). Both the hydroxyl radical and the hole could oxidize TCE and yield TCE degradation products (Eqs. (5) and (6)). The photoinduced hole or the hydroxyl radical could also react with $S_{IV}$ to form the sulfite radical (Eqs. (7) and (8)). The sulfite radicals could then react to degrade TCE (Eqs. (8) and (9)). The electron raised to the conduction band (Eq. (3)) or by $S_{IV}$ direct photolysis (Eq. (10)) could react from the solid or after release to the solution then can reduce TCE (Eqs. (11) and (12)).

$$\mathrm{BiOBr} + \text{solar light} \rightarrow \mathrm{BiOBr}\left(e_{CB}^{-} + h_{VB}^{+}\right) \quad (3)$$

$$h_{VB}^{+} + H_2O \rightarrow {}^{\cdot}OH + H^{+} \quad (4)$$

$$\mathrm{TCE} + {}^{\cdot}OH \rightarrow \text{degradation products (R1)} \quad (5)$$

$$\mathrm{TCE} + h_{VB}^{+} \rightarrow \text{degradation products (R2)} \quad (6)$$

$${}^{\cdot}OH + SO_3^{2-} \rightarrow SO_3^{\cdot -} + OH^{-} \quad (7)$$

$$h_{VB}^{+} + SO_3^{2-} \rightarrow SO_3^{\cdot -} + \mathrm{TCE} \rightarrow \text{degradation products (R3)} \quad (8)$$

$$\mathrm{TCE} + SO_3^{\cdot -} \rightarrow \text{degradation products (R4)} \quad (9)$$

$$SO_3^{2-} + h\nu \rightarrow SO_3^{\cdot -} + e_{aq}^{-} \quad (10)$$

$$\mathrm{TCE} + e_{CB}^{-} \rightarrow \text{degradation products (R5)} \quad (11)$$

$$\mathrm{TCE} + e_{aq}^{-} \rightarrow \text{degradation products (R6)} \quad (12)$$

Based on this discussion, possible photodegradation reactions of TCE over BiOBr photocatalyst are depicted in Scheme 1. TCE can react with hydroxyl radicals (R1) or photoinduced holes (R2), and with sulfite radical produced by reaction with hydroxyl radical or with holes (R3 and R4). Also, the photoinduced electrons can directly react with TCE (R5) or hydrated electrons resulting from $S_{IV}$ photolysis can reduce TCE (R6).

To determine the responsible species for TCE degradation, a series of trapping experiments were conducted

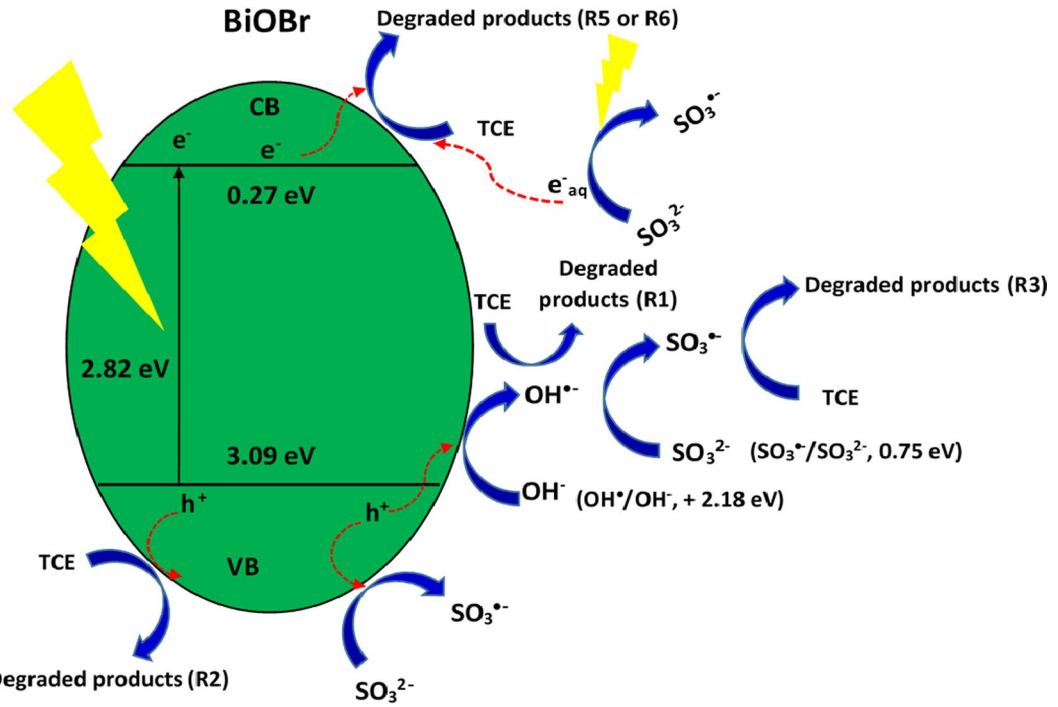


**Scheme 1** Schematic diagram of TCE degradation on the surface of BiOBr photocatalyst with addition of $S_{IV}$ under simulated sunlight irradiation

using potassium iodide (KI) as a hole scavenger, isopropanol (IPA) as hydroxyl radical ($^{\cdot}OH$) scavenger and sodium nitrate as hydrated electron ($e^{-}_{aq}$) scavenger. The conditions in batch experiments using scavengers are shown in Additional file 1: Table S3, Fig. S8 and Fig. S9. Figure 12 compares TCE degradation rates with addition of different scavengers (KI, IPA, and nitrate) for possible active species ($h^{+}$, $^{\cdot}OH$, and $e^{-}_{aq}$). The doses of BiOBr dose and $S_{IV}$ were 1 g/L and 10 mM, respectively. Presence of scavenges had little effect on TCE removal, especially at early times. However, at the end of the experiment TCE concentration was slightly lower in the presence of KI and nitrate, and slightly higher in the presence of IPA. The scavengers probably had little effect because sulfite reacts rapidly with hydroxyl radicals and TCE reacts rapidly with aqueous electron, so they can compete effectively with the scavengers. According to NDRL/NIST data base [50] on the rate constants, average rate constants with hydroxyl radical for $I^{-}$, IPA, and $SO_3^{2-}$ were 1.1E10, 1.6E9, and 5.1E9 ($M^{-1}$ $s^{-1}$) and the rate constant between aqueous electron and TCE was 1.9E10 ($M^{-1}$ $s^{-1}$). Considering the concentrations of reagents, sulfite will have higher rates of reaction with hydroxyl radicals than the scavengers. When the rates are similar, the presence of a scavenger could have some effect, but not a dramatic one. If the reactions occur on the surface, the lack of effect of the scavengers could be due to their adsorbing less effectively on the surface than sulfite and TCE.

In our previous study by Wei et al. [34], batch kinetic experiments were conducted with BiOBr under aerobic conditions to determine if oxidizing radicals such as $SO_4^{\cdot-}$ and $SO_5^{\cdot-}$ were important in MO photodegradation. $SO_4^{\cdot-}$ and $SO_5^{\cdot-}$ are known to be produced from $S_{IV}$ and oxygen via a free radical chain mechanism. As shown in Fig. 13, TCE degradation rate was not greatly affected by the presence of oxygen. The rate constant was estimated to be 0.0212 ($min^{-1}$) in a $N_2$-filled environment and 0.015 ($min^{-1}$) in an aerobic environment. The small change in the rate constant for TCE degradation in the presence of oxygen does not support they hypothesis that $SO_4^{\cdot-}$ and $SO_5^{\cdot-}$ are important species for TCE degradation.

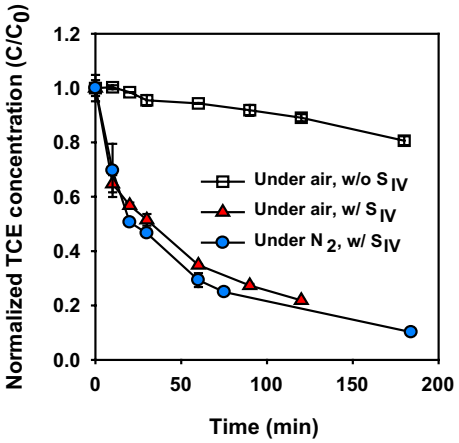


**Fig. 13** Effect of the presence of oxygen on TCE degradation in BiOBr/TCE/$S_{IV}$ system under simulated sunlight. Conditions: $[TCE]_0 = \sim 0.25$ mM, $[SO_3^{2-}]_0 = 2$ mM, BiOBr = 1 g/L, and the solution pH was not buffered

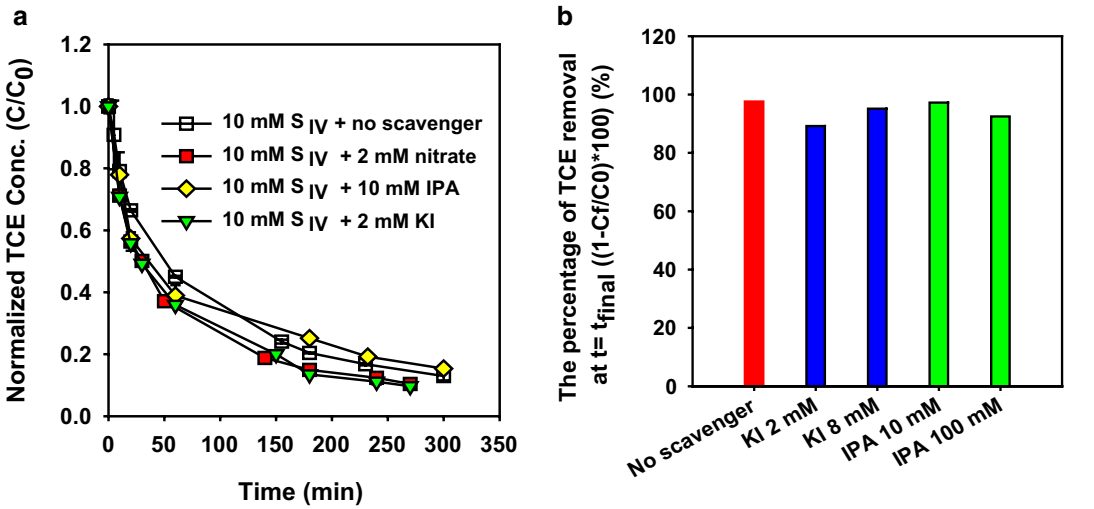


**Fig. 12** Effect of scavengers on TCE degradation (**a**) and comparison of the percentage of TCE removal with different scavengers (**b**) in BiOBr/TCE/$S_{IV}$ system under simulated sunlight. Conditions: **a** $[TCE]_0 = \sim 0.25$ mM, $[SO_3^{2-}] = 10$ mM, and BiOBr = 1 g/L; **b** $[TCE]_0 = \sim 0.25$ mM, $[SO_3^{2-}] = 2$ mM, and BiOBr = 1 g/L. In all experiments, the solution pH was not controlled

It is known that abiotic TCE reductive dechlorination can lead to complete conversion to non-toxic byproducts like acetylene, without the accumulation of less chlorinated compounds such as DCEs, and VC, etc. [51]. In our previous study on TCE degradation in solutions of $S_{IV}$ irradiated by UV light, TCE was almost completely transformed to chloride ion when sufficient $S_{IV}$ was present [40]. Figure 14 shows concentrations of TCE, $S_{IV}$, and chloride ion over irradiation time. As shown in Fig. 14, 92% of initial TCE was degraded after 300 min of simulated sunlight, when the concentrations of BiOBr and $S_{IV}$ were 1 g/L and 10 mM. Rates of TCE removal and chloride formation decreased over the first 120 min. However, some TCE was removed between 120 and 300 min, while no chloride was produced. If it is assumed that all of the initial TCE was completely degraded and formed chloride ion, approximately 0.48 mM of chloride ion would be produced. To quantify the extent of dechlorination, a dechlorination efficiency ($R_{dech}$) was defined as the fraction of chlorine atoms in TCE that was degraded that were converted to chloride ions ($R_{dech} = (C_{Cl,\ at\ t} - C_{Cl,\ at\ t=0})/(C_{Cl,\ initial\ TCE} - C_{Cl,\ final\ TCE})$), where $C_{Cl,\ at\ t}$ is the chloride ion concentration at specific time (mM) and $C_{Cl,\ initial\ TCE}$ and $C_{Cl,\ final\ TCE}$ are the chlorine concentrations (mM) in initial and final TCE, respectively [40]. $R_{dech}$ was measured as 59% after 120 min and 57% after 300 min. Li et al., have studied TCE degradation products by UV photolysis in an aerobic environment. They demonstrated that chloride ions were a major end product and various intermediates including formic acid, di- and mono-chloroacetic acids [22]. If TCE undergoes oxidation in the presence of $O_2$ it could produce $CO_2$ as a final product with various intermediates. In this study, $CO_2$ was detected by gas chromatography with TCD detector after acidifying water sample using 10% $H_3PO_4$. The peak areas of $CO_2$ measured for samples taken at $t = 0$, 20, 60, and 120 min were much less than that of aerated deionized water and the peak area of the sample taken at $t = 300$ min was similar to that of aerated ionized water sample. This shows that little if any $CO_2$ was formed during TCE degradation in the BiOBr/TCE/$S_{IV}$ system under simulated sunlight.

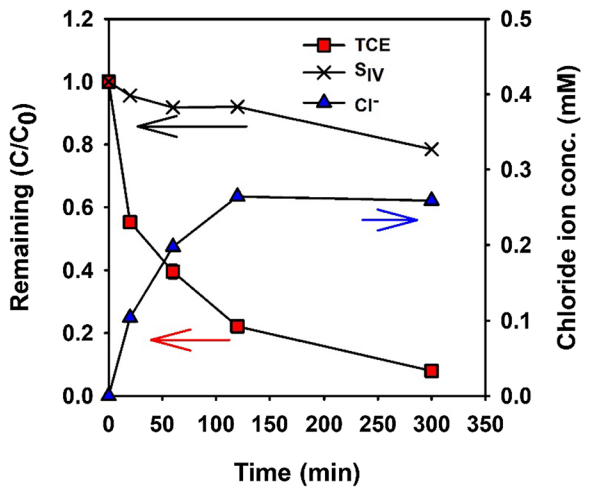


**Fig. 14** Normalized concentration of TCE or $S_{IV}$ species, and formation of chloride ion. Conditions: $[TCE]_0 = \sim 0.16$ mM, $[SO_3^{2-}]_0 = 10$ mM, BiOBr = 1 g/L, and the solution pH was not buffered

We believe that the active species being responsible for TCE degradation in BiOBr/TCE/$S_{IV}$ (photocatalyst/contaminant/reagent) system under simulated solar light is the sulfite radical ($SO_3^{\cdot-}$). This is based on the fact that BiOBr alone did not degrade TCE efficiently and that insufficient doses of $S_{IV}$ limited TCE removal in the presence of BiOBr and light. Our previous study found that the sulfite radical was the active specie for methyl orange degradation in the BiOBr/MO/$S_{IV}$ system under visible light [34]. Furthermore, it was also reported that hydrated electrons and sulfite radicals were active species for TCE degradation with UV-L irradiation [40]. This study showed that scavengers of hydrated electrons did not affect removal of TCE, but did affect the extent to which chloride was produced. This indicates that TCE was being removed by reaction with the sulfite radical and that the product of this reaction was being dechlorinated with hydrated electrons. Finally, it can be concluded that the active specie for TCE degradation is produced from $S_{IV}$ on the surface of BiOBr when irradiated by simulated sunlight. Furthermore, significant TCE degradation was found at weakly acidic pH, which supports the belief that bisulfite also provides the active specie in the $S_{IV}$-promoted photodegradation process.

## Conclusion

Photocatalytic degradation of TCE under simulated solar light using BiOBr nanocomposites was assisted by $S_{IV}$ additions. The remarkable feature is that the active specie for TCE photodegradation is most likely sulfite radical ($SO_3^{\cdot-}$) produced on BiOBr surface by solar irradiation. TCE degradation rate was enhanced by increasing $S_{IV}$ dose till the $S_{IV}$/TCE molar ratio approached 5. TCE degradation rate was also affected by other experimental parameters such as initial TCE concentration, BiOBr dose, and solution pH. The maximum TCE degradation rate was obtained at pH 5.45. A reaction mechanism for TCE degradation over BiOBr was proposed to be as follows: (1) reaction of TCE with hydroxyl radicals or photoinduced holes; (2) reaction with sulfite radical produced by $S_{IV}$ reaction with hydroxyl radical or holes, and (3) reaction with photoinduced electrons or

hydrated electrons. A series of trapping experiments were conducted to determine the responsible specie for TCE degradation in BiOBr/TCE/$S_{IV}$ system. It was found that the scavengers have little effect on the extent and rate of TCE degradation. This was assumed to be due to less effective adsorption of scavengers on the photocatalyst surface than sulfite and TCE. Finally, analysis of degradation products showed that TCE was converted to a non-hazardous chloride and the photocatalytic activity of BiOBr was not affected over a number of treatment cycles when sufficient doses of $S_{IV}$ dose were present. Although sulfite-enhanced photocatalysis using BiOBr for TCE degradation has been successfully demonstrated in this work, various parameters present in water environment that can inhibit or enhance recombination of photoelectrons and holes were not investigated. Further investigations on the effect of dissolved anions including $Cl^-$, $SO_4^{2-}$, $NO_3^-$, $HCO_3^-$, $PO_4^{3-}$ and humic acid or dissolved trace metal cations (e.g., $Cu^{2+}$, $Fe^{3+}$, etc.) on TCE removal in the system of photocatalyst/TCE/reagent are recommended.

## Supplementary information

**Supplementary information** accompanies this paper at https://doi.org/10.1186/s12302-019-0287-9.

**Additional file 1.** Tables and figures.

### Abbreviations

TCE: trichloroethylene; BiOBr: bismuth oxybromide; $S_{IV}$: sulfite; MC: maximum contaminant level; USEPA: United States Environmental Protection Agency; AOPs: advanced oxidation processes; DCAAD: dichloroacetaldehyde; DCAA : dichloroacetic acid; TCAA: trichloroacetic acid; UV: ultraviolet; VB: valence band; MO: methyl orange; RhB: Rhodamine B; DDW: deionized deoxygenated water; SARP: solar light-driven advanced reduction process; GC-μECD: gas chromatograph with a micro-electron capture detector; GC/TCD: gas chromatograph with a thermal conductivity detector; SEM: scanning emission microscope; XRD: X-ray powder diffraction; Ti-BiOX: titanium-doped bismuth oxyhalides; KI: potassium iodide; IPA: isopropanol; $e_{aq}^-$: hydrated electron; $R_{dech}$: dechlorination efficiency.

### Acknowledgements

This paper is based on a project funded by the Qatar National Research Fund under its National Priorities Research Program as 'Solar-driven advanced reduction processes for destroying persistent contaminants in water'.

### Authors' contributions

BJ conducted laboratory experiments, analyzed, interpreted, and evaluated data and drafted the manuscript. WD and YL were responsible for synthesizing and characterizing photocatalysts. BB involved in data analysis and manuscript correction. AA supervised the project and contributed to the interpretation of the results. All authors read and approved the final manuscript.

### Funding

This study was made possible by a grant from the Qatar National Research Fund under its National Priorities Research Program Award Number NPRP 8-1406-2-605. The paper's contents are solely the responsibility of the authors and do not necessarily represent the official views of the Qatar National Research Fund.

### Availability of data and materials

The datasets used and analyzed during the current study are available from the corresponding author on reasonable request.

### Ethics approval and consent to participate

Not applicable.

### Consent for publication

All authors agreed to publish the paper.

### Competing interests

The authors declare that they have no competing interests.

### Author details

[1] Chemical Engineering Program, Texas A&M University at Qatar, Education City, P.O. Box 23874, Doha, Qatar. [2] Department of Mechanical Engineering, Texas A&M University, College Station, TX, USA. [3] Department of Civil Engineering, Texas A&M University, College Station, TX, USA.

Received: 18 September 2019 Accepted: 29 December 2019
Published online: 29 January 2020

### References

1. USEPA (2017) Risk management for trichloroethylene (TCE). In: Assessing and managing chemicals under TSCA. United States Environmental Protection Agency. https://www.epa.gov/assessing-and-managing-chemicals-under-tsca/risk-management-trichloroethylene-tce. Accessed 2019
2. Fan J, Yates JT (1996) Mechanism of photo-oxidation of trichloroethylene on $TiO_2$: detection of intermediates by infrared spectroscopy. J Am Chem Soc 118:4686–4692
3. Yamazaki-Nishida S, Cervera-March S, Nagano KJ, Anderson MA, Hori K (1995) Experimental and theoretical study of the reaction mechanism of the photoassisted catalytic degradation of trichloroethylene in the gas phase. J Phys Chem 99:15814–15821
4. USEPA (1997) Use of monitored natural attenuation at superfund, RCRA corrective action, and underground storage tank sites. Directive No. 9200.4-17P. Office of Solid Waste and Emergency Response. Washington DC, USA
5. Russel HH, Matthews JE, Sewell GW (1992) Groundwater issue: TCE removal from contaminated soil and groundwater. No: EPA/540/S-92/002. Washington DC, USA
6. Vogel TM, Criddle CS, McCarty PL (1987) Transformation of halogenated aliphatic compounds. Environ Sci Technol 21:722–736
7. Pant P, Pant S (2010) A review: advances in microbial remediation of trichloroethylene (TCE). J Environ Sci 22:116–126
8. Yang GCC, Liu C-Y (2001) Remediation of TCE contaminated soils by in situ EK-fenton process. J Hazard Mater 85:317–331
9. Esplugas S, Giménez J, Contreras S, Pascual E, Rodríguez M (2002) Comparison of different advanced oxidation processes for phenol degradation. Water Res 36:1034–1042
10. Hirvonen A, Tuhkanen T, Kalliokoski P (1996) Formation of chlorinated acetic acids during UV/$H_2O_2$-oxidation of ground water contaminated with chlorinated ethylenes. Chemosphere 32:1091–1102
11. Hirvonen A, Tuhkanen T, Kalliokoski P (1996) Treatment of TCE- and PCE contaminated groundwater using UV/$H_2O_2$ and $O_3$/$H_2O_2$ oxidation process. Water Sci Technol 33:67–73
12. Wang D, Bolton JR, Hofmann R (2012) Medium pressure UV combined with chlorine advanced oxidation for trichloroethylene destruction in a model water. Water Res 46:4677–4686
13. Li K, Stefan MI, Crittenden JC (2004) UV photolysis of trichloroethylene: product study and kinetic modeling. Environ Sci Technol 38:6685–6693
14. Chu W, Jia J (2009) The photodegradation and modeling of a typical NAPL, trichloroethylene by monochromatic UV irradiations. Environ Sci Technol 43:1455–1459
15. Pruden AL, Ollis DF (1983) Photoassisted heterogeneous catalysis: the degradation of trichloroethyelene in water. J Catal 82:404–417
16. Phillips LA, Raupp GB (1992) Infrared spectroscopic investigation of gas-solid heterogeneous photocatalytic oxidation of trichloroethylene. J Mol Catal 77:297–311

17. Glaze WH, Kenneke JF, Ferry JL (1993) Chlorinated byproducts from the $TiO_2$-mediated photodegradation of trichloroethylene and tetrachloroethylene in water. Environ Sci Technol 27:177–184
18. Sun H, Zhou G, Liu S, Ang HM, Tadé MO, Wang S (2013) Visible light responsive titania photocatalysts codoped by nitrogen and metal (Fe, Ni, Ag, or Pt) for remediation of aqueous pollutants. Chem Eng J 231:18–25
19. Asahi R, Morikawa T, Ohwaki T, Aoki K, Taga Y (2001) Visible-light photocatalysis in nitrogen-doped titanium oxides. Science 293:269–271
20. Zhao J, Chen C, Ma W (2005) Photocatalytic degradation of organic pollutants under visible light irradiation. Top Catal 35:269–278
21. Li Z, Fang Y, Zhan X, Xu S (2013) Facile preparation of squarylium dye sensitized $TiO_2$ nanoparticles and their enhanced visible-light photocatalytic activity. J Alloy Compd 564:138–142
22. Xu Y-S, Yu Y-X, Zhang W-D (2014) Wide bandgap $Bi_2O_2CO_3$-coupled $Bi_2MoO_6$ heterostructured hollow microspheres: one-pot synthesis and enhanced visible-light photocatalytic activity. J Nanosci Nanotechnol 14:6800–6809
23. Fu H, Xu T, Zhu S, Zhu Y (2008) Photocorrosion inhibition and enhancement of photocatalytic activity for ZnO via hybridization with C60. Environ Sci Technol 42:8064–8069
24. Ganose AM, Cuff M, Butler KT, Walsh A, Scanlon DO (2016) Interplay of orbital and relativistic effects in bismuth oxyhalides: BiOF, BiOCl, BiOBr, and BiOI. Chem Mater 28:1980–1984
25. Cheng H, Huang B, Dai Y (2014) Engineering BiOX (X=Cl, Br, I) nanostructures for highly efficient photocatalytic applications. Nanoscale 6:2009–2026
26. Jia X, Cao J, Lin H, Zhang M, Guo X, Chen S (2017) Transforming type-I to type-II heterostructure photocatalyst via energy band engineering: a case study of I-BiOCl/I-BiOBr. Appl Catal B 204:505–514
27. Dandapat A, Gnayem H, Sasson Y (2016) The fabrication of BiOClxBr 1–x/alumina composite films with highly exposed 001 facets and their superior photocatalytic activities. Chem Commun 52:2161–2164
28. Gao S, Guo C, Hou S, Wan L, Wang Q, Lv J, Zhang Y, Gao J, Meng W, Xu J (2017) Photocatalytic removal of tetrabromobisphenol A by magnetically separable flower-like BiOBr/BiOI/$Fe_3O_4$ hybrid nanocomposites under visible-light irradiation. J Hazard Mater 331:1–12
29. Zhang X, Wang C-Y, Wang L-W, Huang G-X, Wang W-K, Yu H-Q (2016) Fabrication of $BiOBrxI_{1-x}$ photocatalysts with tunable visible light catalytic activity by modulating band structures. Sci Rep 6:22800
30. Chai SY, Kim YJ, Jung MH, Chakraborty AK, Jung D, Lee WI (2009) Heterojunctioned BiOCl/$Bi_2O_3$, a new visible light photocatalyst. J Catal 262:144–149
31. Cheng H, Huang B, Wang P, Wang Z, Lou Z, Wang J, Qin X, Zhang X, Dai Y (2011) In situ ion exchange synthesis of the novel Ag/AgBr/BiOBr hybrid with highly efficient decontamination of pollutants. Appl Surf Sci 47:7054–7056
32. Di J, Xia J, Ji M, Wang B, Yin S, Zhang Q, Chen Z, Li H (2016) Advanced photocatalytic performance of graphene-like BN modified BiOBr flower-like materials for the removal of pollutants and mechanism insight. Appl Catal B 183:254–262
33. Wang S, Yang X, Zhang X, Ding X, Yang Z, Dai K, Chen H (2017) A plate-on-late sandwiched Z-scheme heterojunction photocatalyst: BiOBr-$Bi_2MoO_6$ with enhanced photocatalytic performance. Appl Surf Sci 391:194–201
34. Deng W, Zhao H, Pan F, Feng X, Jung B, Abdel-Wahab A, Batchelor B, Li Y (2017) Visible-light-driven photocatalytic degradation of organic water pollutants promoted by sulfite addition. Environ Sci Technol 51:13372–13379
35. Li Y, Wang Z, Huang B, Dai Y, Zhang X, Qin X (2015) Synthesis of BiOBr-PVP hybrids with enhanced adsorption-photocatalytic properties. Appl Surf Sci 347:258–264
36. Norman ROC, Storey PM (1971) Electron spin resonance studies Part XXXI The generation, and some reactions, of the radicals $SO_3^-$ ˙, $S_2O_3^-$ ˙, $S^{-}$, and SH in aqueous solution. J Chem Soc B Phys Org 0:1009–1013
37. Ozawa T, Kwan T (1983) Esr studies on the reactive character of the radical anions, $SO_2^-$, $SO_3^-$ and $SO_4^-$ in aqueous solution. Polyhedron 2:1019–1023
38. Erben-Russ M, Bors W, Winter R, Saran M (1986) The reaction of sulfite anion radical ($SO^{-3}$) with polyunsaturated fatty acids. Int J Radiat Appl Instrum Part C Radiat Phys Chem 27:419–424
39. Huie RE, Neta P (1984) Chemical behavior of sulfur trioxide (1-)($SO_3^-$) and sulfur pentoxide (1-)($SO_5^-$) radicals in aqueous solutions. J Phys Chem 88:5665–5669
40. Jung B, Farzaneh H, Khodary A, Abdel-Wahab A (2015) Photochemical degradation of trichloroethylene by sulfite-mediated UV irradiation. J Environ Chem Eng 3:2194–2202
41. Liu X, Yoon S, Batchelor B, Abdel-Wahab A (2013) Degradation of vinyl chloride (VC) by the sulfite/UV advanced reduction process (ARP): effects of process variables and a kinetic model. Sci Total Environ 454–455:578–583
42. Deng W, Pan F, Batchelor B, Jung B, Zhang P, Abdel-Wahab A, Zhoud H, Li Y (2019) Mesoporous $TiO_2$–BiOBr microspheres with tailorable adsorption capacities for photodegradation of organic water pollutants: probing adsorption–photocatalysis synergy by combining experiments and kinetic modeling. Environ Sci Water Res Technol 5:769–781
43. Neta P, Huie RE, Ross AB (1988) Rate constants for reactions of inorganic radicals in aqueous solution. J Phys Chem Ref Data 17:1027–1284
44. Waygood SJ, McElroy WJ (1992) Spectroscopy and decay kinetics of the sulfite radical anion in aqueous solution. J Chem Soc Faraday Trans 88:1525–1530
45. Zhang Y, Park M, Kim HY, Ding B, Park S-J (2016) In-situ synthesis of nanofibers with various ratios of $BiOCl_x$/$BiOBr_y$/$BiOI_z$ for effective trichloroethylene photocatalytic degradation. Appl Surf Sci 384:192–199
46. Fujishima A, Zhang XT, Tryk DA (2008) $TiO_2$ photocatalysis and related surface phenomena. Surf Sci Rep 63:515–582
47. Liu X, Yoon S, Batchelor B, Abdel-Wahab A (2013) Photochemical degradation of vinyl chloride with an advanced reduction process (ARP)-effects of reagents and pH. Chem Eng J 215–216:868–875
48. Jung B, Nicola R, Batchelor B, Abdel-Wahab A (2014) Effect of low- and medium-pressure Hg UV irradiation on bromate removal in advanced reduction process. Chemosphere 117:663–672
49. Liu W, Yang Q, Wang Z, Lv X, Yang Z (2018) Photocatalytic degradation of trichloroethylene over BiOCl under UV irradiation. Appl Organomet Chem 32:e4354
50. NIST (2002) Notre Dame Radiation Laboratory/National Institute of Standards and Technology (NDRL/NIST) solution kinetics database on the web, https://kinetics.nist.gov/solution/. Accessed Dec 2018
51. Butler E, Dong Y, Liang X, Kuder T, Philp RP, Krumholz LR (2009) Abiotic reductive dechlorination of tetrachloroethylene and trichloroethylene in anaerobic environments. University of Oklahoma, Norman


## Publisher's Note